European Journal of Medicinal Chemistry 151 (2018) 186–198

Contents lists available at ScienceDirect

European Journal of Medicinal Chemistry

journal homepage: http://www.elsevier.com/locate/ejmech

Research paper

Repositioning of the antipsychotic trifluoperazine: Synthesis, biological evaluation and *in silico* study of trifluoperazine analogs as anti-glioblastoma agents

Seokmin Kang [a, 1], Jung Moo Lee [b, c, 1], Borami Jeon [d, 1], Ahmed Elkamhawy [d, e], Sora Paik [d, f], Jinpyo Hong [c], Soo-Jin Oh [c, g], Sun Ha Paek [h], C. Justin Lee [b, c, i], Ahmed H.E. Hassan [j], Sang Soo Kang [a, *], Eun Joo Roh [d, i, **]

[a] Department of Anatomy and Convergence Medical Science, Institute of Health Sciences, College of Medicine, Gyeongsang National University, Jinju, 52727, Republic of Korea
[b] KU-KIST Graduate School of Converging Science and Technology, Korea University, Seoul, 02841, Republic of Korea
[c] Center for Neuroscience and Functional Connectomics, Brain Science Institute, Korea Institute of Science and Technology, Seoul, 02792, Republic of Korea
[d] Chemical Kinomics Research Center, Korea Institute of Science and Technology, Seoul, 02792, Republic of Korea
[e] Department of Pharmaceutical Organic Chemistry, Faculty of Pharmacy, Mansoura University, Mansoura, 35516, Egypt
[f] Department of Fundamental Pharmaceutical Sciences, College of Pharmacy, Kyung Hee University, Seoul, 02447, Republic of Korea
[g] Convergence Research Center for Diagnosis, Treatment and Care System of Dementia, Korea Institute of Science and Technology, Seoul, 02792, Republic of Korea
[h] Department of Neurosurgery, College of Medicine, Seoul National University, Seoul, 08826, Republic of Korea
[i] Division of Bio-Medical Science & Technology, KIST School, Korea University of Science and Technology, Seoul, 02792, Republic of Korea
[j] Department of Medicinal Chemistry, Faculty of Pharmacy, Mansoura University, Mansoura, 35516, Egypt

ARTICLE INFO

Article history:
Received 27 November 2017
Received in revised form
18 March 2018
Accepted 19 March 2018
Available online 23 March 2018

Keywords:
Trifluoperazine
Trifluoperazine analogs
Brain cancer
Glioblastoma
Calcium
Orthotopic brain xenograft mouse model

ABSTRACT

Repositioning of the antipsychotic drug trifluoperazine for treatment of glioblastoma, an aggressive brain tumor, has been previously suggested. However, trifluoperazine did not increase the survival time in mice models of glioblastoma. In attempt to identify an effective trifluoperazine analog, fourteen compounds have been synthesized and biologically *in vitro* and *in vivo* assessed. Using MTT assay, compounds **3dc** and **3dd** elicited 4–5 times more potent inhibitory activity than trifluoperazine with $IC_{50} = 2.3$ and 2.2 μM against U87MG glioblastoma cells, as well as, $IC_{50} = 2.2$ and 2.1 μM against GBL28 human glioblastoma patient derived primary cells, respectively. Furthermore, they have shown a reasonable selectivity for glioblastoma cells over NSC normal neural cell. *In vivo* evaluation of analog **3dc** confirmed its advantageous effect on reduction of tumor size and increasing the survival time in brain xenograft mouse model of glioblastoma. Molecular modeling simulation provided a reasonable explanation for the observed variation in the capability of the synthesized analogs to increase the intracellular Ca^{2+} levels. In summary, this study presents compound **3dc** as a proposed new tool for the adjuvant chemotherapy of glioblastoma.

1. Introduction

Glioblastoma is the most prevalent and devastating primary malignant tumor of the brain [1,2]. It is characterized by very poor prognosis with median survival time of 14–16 months in patients, as well as, a very low 5-years survival rate of only 9.8% [3–6]. Because of its location within the CNS, rapid proliferative rate, resistance to apoptosis, and aggressive invasive cellular property, glioblastoma therapy is very challenging [1,7–9]. Up-to-date, temozolomide (TMZ, **1**, Fig. 1) is the major drug of choice for the first line treatment of glioblastoma according to the European Organization for Research and Treatment of Cancer (EORTC) and the Radiation Therapy Oncology Group (RTOG) [10]. TMZ is a prodrug whose core, the imidazotetrazine ring,

* Corresponding author.
** Corresponding author. Chemical Kinomics Research Center, Korea Institute of Science and Technology, Seoul, 02792, Republic of Korea.
E-mail addresses: kangss@gnu.ac.kr (S.S. Kang), r8636@kist.re.kr (E.J. Roh).
[1] Authors contributed equally to this work.

https://doi.org/10.1016/j.ejmech.2018.03.055
0223-5234/

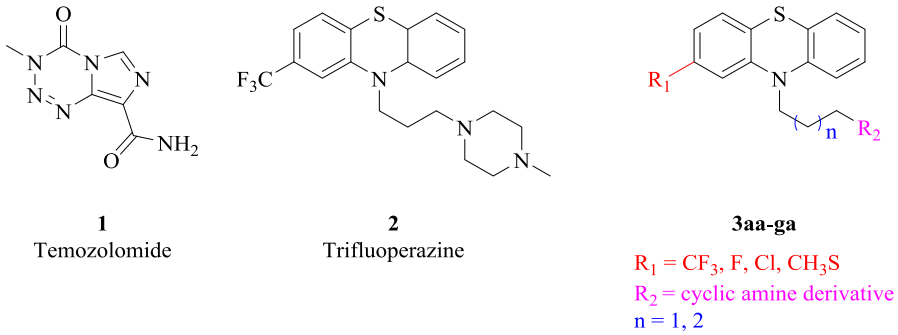

Fig. 1. Structures of TMZ (**1**), TFP (**2**) and the designed ligands (**3**).

undergoes spontaneous hydrolysis at the physiologic pH to produce 5-(3-methyltriazen-1-yl)imidazole-4-carboxamide (MTIC) which acts as an alkylating agent delivering a methyl group to DNA bases [11]. Unfortunately, more than 50% of TMZ-treated glioblastoma patients do not show effective response to TMZ, may be because of TMZ resistant glioblastoma cells [12,13]. In addition, the average increase in the life span of TMZ-treated glioblastoma patients is estimated to be around only 2.5 months with high tumor relapse [5,11,14–16]. Despite the introduction of novel surgical procedures, radiation techniques and adjuvant chemotherapeutic agents, the efficient treatment of glioblastoma is still lacking [1,5,17].

Recently, repositioning or repurposing of the approved drugs for treatment of diseases other than their known indications has gained the attention of the scientific society [18,19]. Because of the proven safety and quality of the drugs already available on the market, the process of drug repositioning could save much time, efforts and costs that would be invested in the discovery and development of novel chemical entities [19,20].

Repositioning of trifluoperazine (TFP, **2**, Fig. 1); a well-known antipsychotic drug for treatment of schizophrenia, has been explored as chemotherapeutic agent against several tumors including lung cancer [21], breast cancer, [22,23] and T-cell lymphoma [24]. In addition, it has been reported that TFP could inhibit glioblastoma cells' proliferation, migration, and invasion [5]. A mechanistic study revealed that the anti-glioblastoma activity of TFP is mediated through increasing the intracellular Ca^{2+} level *via* opening of inositol 1,4,5-trisphosphate receptor (IP_3R) subtype 1 and 2 which is the result of the induced dissociation of calmodulin (CaM) subtype 2 from IP_3R [5]. However, *in vivo* TFP-treated brain xenograft mouse model showed no increase in the survival time [5]. TFP analogs inducing more elevated intracellular Ca^{2+} levels could result in better biological response. The reported crystal structures for TFP bound to CaM show different binding modes within the hydrophobic cleft C-domain of CaM (Protein Databank codes: 1LIN and 1CTR) [25]. In the crystal structure 1LIN, the trifluoromethyl moiety is buried within the hydrophobic pocket which is not the case in the crystal structure 1CTR. Also, the cyclic amine; methylpiperazinyl moiety contributes to the binding by forming favorable interactions with residues within its vicinity. Exploration of the chemical space in the vicinity of TFP through modification of the trifluoromethyl and the cyclic amine moieties, as well as the length of the alkyl chain linker connecting the cyclic amine moiety with the core phenothiazine ring might provide TFP analogs **3aa**–**3ga** (Fig. 1) eliciting more increased intracellular Ca^{2+} level. Thus, these analogs might be more effective chemotherapeutic agents possessing significant *in vivo* increased survival time.

2. Results and discussion

2.1. Chemistry

A concise synthesis of the targeted TFP analogs (**3aa**–**ga**) was performed in two synthetic steps starting from commercially available phenothiazine derivatives **4a**–**d** (Scheme 1). First, deprotonation of phenothiazine derivatives **4a**–**d** with NaH (60% in oil) followed by S_N2 nucleophilic substitution reaction with 1,3- or 1,4-dihaloalkane at 100 °C for 24 h afforded the *N*-alkylated intermediates **5a**–**g** in 95–25.6% isolated yields. In the second step, the chloro group in intermediates **5a**–**g** has been displaced with the appropriate cyclic amine derivative *via* S_N2 reaction using NaI as a reaction promoter and K_2CO_3 as a base at 80 °C for 24 h to yield the desired TFP analogs (**3aa**–**ga**). Accordingly, new fourteen TFP analogs were prepared and submitted for biological evaluation.

2.2. Evaluation of Ca^{2+} imaging

Intracellular Ca^{2+} signaling is important for gene expression, migration, invasion, and survival of glioblastoma cells [4]. TFP has been reported to inhibit the proliferation and invasion of glioblastoma by increasing the intracellular Ca^{2+} release [5]. Consequently, TFP analogs capable of eliciting more intracellular Ca^{2+} increase relative to TFP could possess an enhanced antitumor effect against glioblastoma cells. Accordingly, the ability of the newly synthesized TFP analogs to increase the intracellular Ca^{2+} was evaluated by measuring the intracellular Ca^{2+} in U87MG glioblastoma cells. The results (Table 1) were calculated as percent of the increase of the intracellular Ca^{2+} produced by TFP.

First, TFP analog **3aa** having no *N*-methyl group in the piperazine moiety was synthesized and evaluated. This analog elicited 8% higher increase in the intracellular Ca^{2+} than that of TFP. Replacement of the 4-methylpiperazinyl with 4-(pyrrolidinyl)-piperidinyl (two cyclic amine moities linked together) afforded analog **3ab** which elicited an increase in the intracellular Ca^{2+} lower by 28% relative to that of TFP. Also, replacement of the 4-methylpiperazinyl with 4-methylpiperidinyl which has only one nitrogen atom resulted in analog **3ac** which also showed a less increase of intracellular Ca^{2+} relative to TFP. Modification of the trifluoromethyl and the cyclic amine moieties into chloro group and 4-methylpiperidinyl moiety respectively afforded analog **3ba** which elicited a lower increase of intracellular Ca^{2+} relative to TFP but higher than analog **3ac**. However, analog **3ca** possessing methylthio and 4-methylpiperidinyl moieties elicited even a lower level of intracellular Ca^{2+}. Next, analogs with increased length of the alkyl chain linker connecting the cyclic amine moiety with the phenothiazine scaffold were explored. Analog **3da** possessing 4-methylpiperidinyl moiety elicited a little decrement in the ability

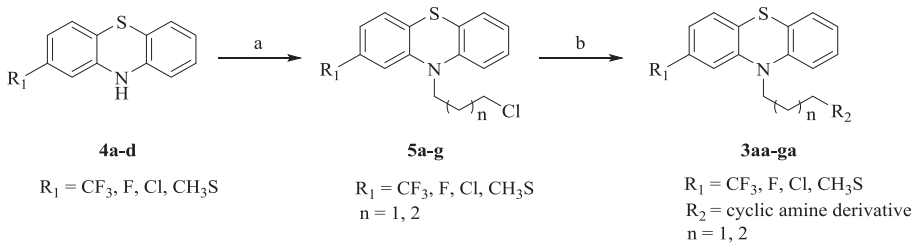

Scheme 1. Reagents and conditions: (a) 1,3- or 1,4-dihaloalkane, NaH (60% in oil), DMF, 100 °C, 24 h; (b) appropriate cyclic amine, NaI, K_2CO_3, 2-butanone, 80 °C, 24 h.

Table 1
Structure and Ca^{2+} response of TFP and the newly synthesized analogs.

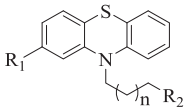

Comp	n	R_1	R_2	[a]Activation (%)	Comp	n	R_1	R_2	[a]Activation (%)
3aa	1	CF_3		108	**3dd**	2	CF_3	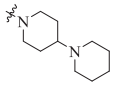	123
3ab	1	CF_3	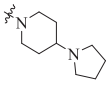	72	**3de**	2	CF_3		94
3ac	1	CF_3		83	**3df**	2	CF_3		107
3ba	1	Cl		88	**3ea**	2	F		110
3ca	1	CH_3S		76	**3fa**	2	CH_3S		72
3da	2	CF_3		93	**3ga**	2	Cl	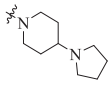	101
3db	2	CF_3	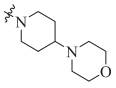	120	**TFP**	1	CF_3		100
3dc	2	CF_3	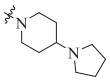	134					

[a] Activation; Ca^{2+} response (% of trifluoperazine).

to increase the intracellular Ca^{2+} relative to TFP. Analog **3ea** possessing the electron withdrawing fluoro group and analog **3fa** having the electron donating methylthio moiety, as well as, 4-methylpiperidinyl moiety and the one carbon extended linker elicited an increase in intracellular Ca^{2+} higher and lower by 10% and 28% respectively relative to that of TFP. Notably, TFP analogs **3db**, **3dc** and **3dd** possessing the two cyclic amine moities linked together, an extended linker, and trifluoromethyl moiety elicited a significant increase in the intracellular Ca^{2+} (20%, 34% and 23% higher increase in intracellular Ca^{2+} than that of TFP, respectively). Replacement of the two linked cyclic amine moities in these derivatives with 4-phenylpiperazinyl moiety to afford analog **3de** did not result in any significant increase of intracellular Ca^{2+} relative to TFP, while replacement of the two cyclic amine moieties with 4-methyl-1,4-diazepanyl moiety elicited only 7% higher increase in intracellular Ca^{2+} relative to TFP. Replacement of trifluoromethyl moiety in the most effective analog **3dc** with chloro group afforded analog **3ga** possessing an efficacy equivalent to that of TFP. Among the synthesized compounds, analogs **3db**, **3dc** and **3dd** (Fig. 2A), which had a tendency to exhibit more intracellular Ca^{2+} increase than TFP in glioblastoma cells, were selected and further tested by performing additional Ca^{2+} imaging experiment. We found that 100 μM of **3dc** and **3dd** significantly increased the intracellular Ca^{2+} compared to same concentration of TFP on U87MG cells (Fig. 2B and C). In contrast to analogs **3dc** and **3dd**, the Ca^{2+} response exerted by analog **3db** had no significant difference compared to TFP, although there was a tendency to increase more intracellular Ca^{2+} than TFP (Fig. 2B and C).

To check the potency and efficacy of TFP, as well as, the three TFP analogs **3db**, **3dc** and **3dd** in terms of Ca^{2+} response in U87MG cells,

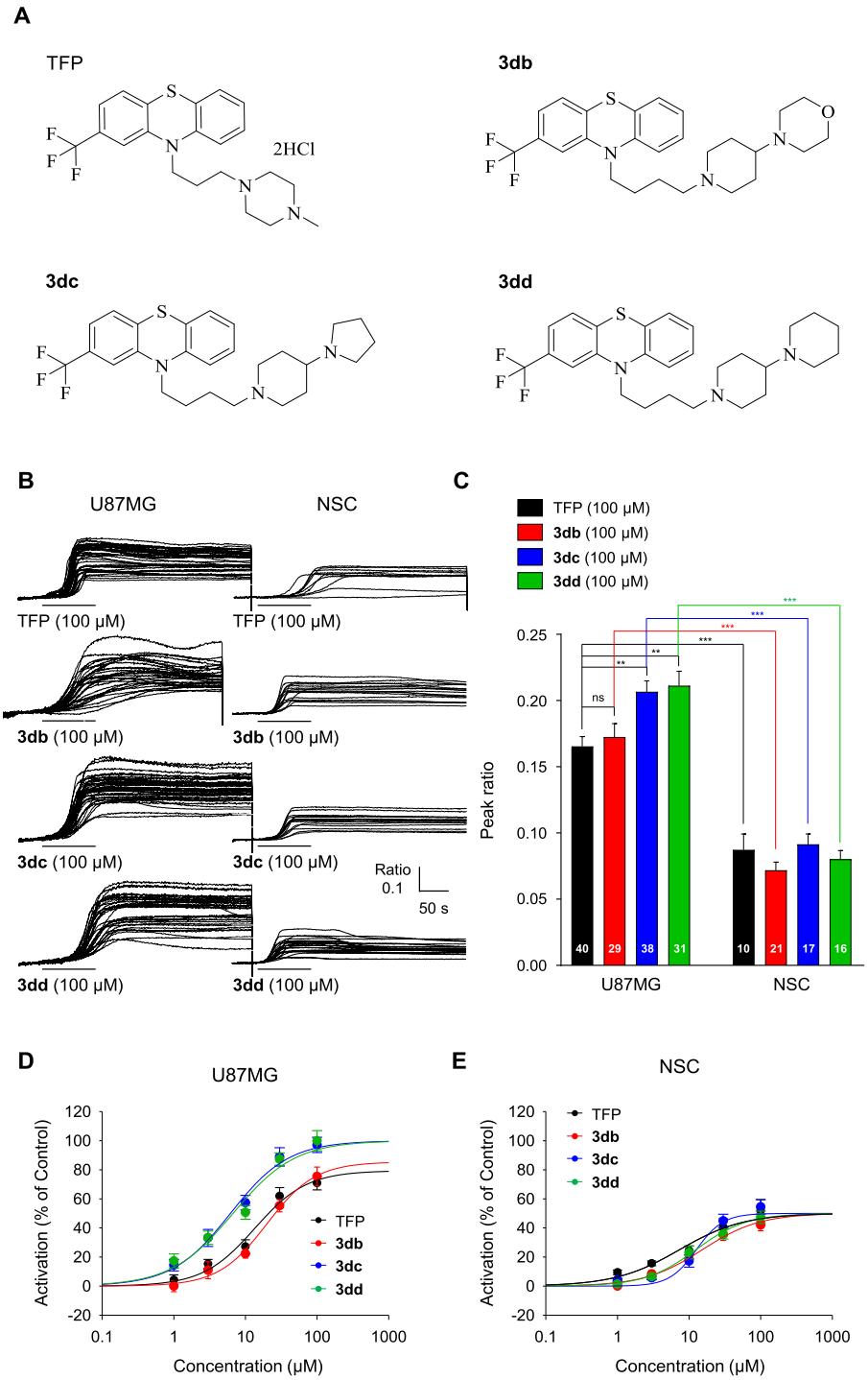

Fig. 2. Intracellular Ca^{2+} increase by TFP, **3db**, **3dc**, and **3dd** in U87MG glioblastoma cells and neural stem cells. (A) Structure of TFP, **3db**, **3dc**, and **3dd**. (B) Ca^{2+} imaging traces of TFP, **3db**, **3dc** and **3dd** at the concentration of 100 μM in U87MG or NSC. Black horizontal bars indicate time and duration of TFP or TFP analogs application. (C) Ca^{2+} peak amplitude from B. Asterisk indicates a significant difference determined by two-way ANOVA (ns, not significant; $^{**}p < 0.01$; $^{***}p < 0.001$). Number on each bar refers to the number of cells. (D and E) Dose response curves from TFP or three of TFP analogs-induced Ca^{2+} peak amplitude under several concentrations (1, 3, 10, 30 and 100 μM) in U87MG cells (D) and NSCs (E). The number of U87MG cells in each concentrations of drugs (1, 3, 10, 30 and 100 μM); TFP ($n = 33, 40, 33, 28, 40$), **3db** ($n = 33, 24, 33, 34, 29$), **3dc** ($n = 43, 28, 48, 38, 38$), **3dd** ($n = 34, 30, 48, 60, 31$). The number of NSCs in each concentrations of drugs; TFP ($n = 12.\ 10, 18, 13, 10$), **3db** ($n = 10, 20, 18, 14, 21$), **3dc** ($n = 18, 19, 15, 14, 17$), **3dd** ($n = 18, 17, 15, 15, 16$).

we measured the intracellular Ca^{2+} increase under several concentrations (1, 3, 10, 30 and 100 μM). As a result, we found that EC_{50} of **3dc** (6.2 μM) and **3dd** (6.7 μM) was half of that of TFP (13.5 μM) in U87MG cells (Fig. 2D). However, **3db** had higher EC_{50} (19.9 μM) than TFP (13.5 μM). Moreover, the efficacy of **3dc** (100%) and **3db** (100%) is higher than that of TFP (79%) and **3db** (85%) (Fig. 2D). Since these results indicate that **3dc** and **3dd** are more potent and effective than TFP as enhancers of intracellular Ca^{2+} in U87MG cells, they might exert cytotoxic effect better than TFP on glioblastoma cells.

Next, we examined whether the effect of TFP and the three TFP analogs **3db**, **3dc** and **3dd** on intracellular Ca^{2+} is specific to

glioblastoma cells but not to normal cells. We further performed Ca^{2+} imaging to measure the tested compounds-induced Ca^{2+} response in NSCs. It was found that Ca^{2+} response by 100 μM of TFP, **3db**, **3dc** or **3dd** in control neural stem cells (NSCs) was significantly lower than that in U87MG cells (Fig. 2B and C). We also measured the Ca^{2+} response under several concentrations (1, 3, 10, 30 and 100 μM) of the tested compounds in NSCs at the same time used for U87MG cells. As a result, analogs **3dc** and **3db** showed 2-fold higher efficacy (100%) in glioblastoma cells than that in normal cells (50%) (Fig. 2D and E). These results indicated that **3db**, **3dc**, **3dd** and TFP are more effective in glioblastoma cells than normal cells. This might predict a desirable selectivity of these compounds for glioblastoma cells over normal cells.

2.3. In vitro anti-glioblastoma activity

MTT cell viability was used to determine whether the increased intracellular Ca^{2+} induced by TFP analogs **3db**, **3dc**, and **3dd** would improve the inhibitory action of TFP on glioblastoma cell growth. Glioblastoma cell lines U87MG, GBL28 as well as, the NSC were used. While the significant decrease of U87MG cell viability started from 5 μM concentration of TFP and **3db**, concentration, as low as, 2 μM of analogs **3dc** and **3dd** significantly decreased the U87MG cell viability (Fig. 3A). The determined IC_{50} values were 2.3 and 2.2 μM for **3dc** and **3dd**, respectively (Fig. 3D and Table 2). In comparison with TFP and **3db** whose IC_{50} values of their anti-glioblastoma effect were 9.9 and 7.1 μM respectively, analogs **3dc** and **3dd** possessed 4–5 times higher potency than TFP on U87MG cells.

The potent anti-glioblastoma activity of analogs **3dc** and **3dd** was further elucidated against the human primary glioblastoma GBL28 cell line. The 1 μM concentration of analogs **3dc** and **3dd** significantly reduced the MTT cell viability of GBL28 cell viability with determined IC_{50} of 2.2 and 2.1 μM respectively, whereas TFP affected the GBL28 cell viability starting from 5 μM concentration (Fig. 3B) with an IC_{50} of 10.2 μM (Fig. 3D and Table 2). On the other hand, analog **3db** elicited a significant reduction of viability starting from 2 μM with IC_{50} of 6.5 μM. Accordingly, analogs **3dc** and **3dd** were the more potent compounds having about 4–5 fold enhanced potency compared with TFP on GBL28 cells (Table 2).

The selectivity of elicited cytotoxic effect of the evaluated compound was checked against NSCs; MTT assay was performed to measure the NSC viability using TFP and the three analogs **3db**, **3dc** and **3dd**. Analog **3dc** significantly inhibited the NSC viability starting from 5 μM concentration with an elicited inhibition efficacy equals to 45%, which was around the half inhibition efficacy values elicited by **3dc** in U87MG and GBL28 glioblastoma cell line that were 82% and 85% respectively (Fig. 3D and Table 2). Similarly, the elicited viability inhibition efficacy of analog **3dd** in NSCs was also about half of that in U87MG and GBL28 cell lines, while for TFP and analog **3db** it was around one quarter of that in U87MG and GBL28 cell lines (Fig. 3D and Table 2). As a whole, relative to TFP and analog **3db**, analogs **3dc** and **3dd** possess more potent anti-glioblastoma activity and reasonable selective cytotoxicity for glioblastoma over normal cell lines.

2.4. In vivo study of *3dc* in the orthotopic brain xenograft mouse model

After assessment of the *in vitro* anti-glioblastoma activity, the potent analog **3dc** which has shown the highest increase in the intracellular Ca^{2+} level was evaluated in an *in vivo* orthotopic brain xenograft mouse model. For establishment of the *in vivo* model, U87MG cells were implanted into the brain of athymic mice (BALB/C nu/nu) *via* intracranial injection. After 3 days of implantation, 0.9% saline (control, $n = 10$) or analog **3dc** (5 mg/kg/day) ($n = 10$) were intraperitoneally administrated for 21 days after which, administration was discontinued till day 39 when surviving animals were scarified and pathohistologically examined (Fig. 4A). Mice were monitored daily for their general appearance, behavioral changes, and neurologic deficits to detect any potential side effects that might be triggered (if any) by **3dc** such as Parkinsonism and extrapyramidal side effect (EPS). No sign of such side effects has been detected after injecting analog **3dc** during the conduction of the described experiment.

Staining of the mice brain with hematoxylin and eosin (H&E) to measure the tumor size showed that administration of **3dc** significantly reduced the tumor size by around 88% relative to the control mice (Fig. 4B and C). Furthermore, the survival of **3dc**-treated brain xenografts mice has increased by 6 days relative to that the control group (Fig. 4D). Previously we demonstrated that TFP reduced 75% of tumor size but showed no increase of the survival time of orthotopic brain xenograft mice [5]. Hence, analog **3dc** might be a better tool than TFP showing an enhanced *in vitro* and *in vivo* anti-glioblastoma activity and increased survival time of orthotopic brain xenograft mouse model of glioblastoma.

2.5. Molecular modeling study

TFP has been shown to elicit anti-glioblastoma activity *via* binding to Calmodulin (CaM) [5]. Investigation of the reported co-crystal structures of TFP-CaM complex reveals that TFP binds to two distinctive hydrophobic binding pockets in the C-domain and the N-domain of CaM [26]. The variable 1:1, 1:2 and 1:4 ratios of CaM:TFP respectively have been reported within several resolved crystal structures. The crystal structure (PDB code 1LIN); whose ratio is 1:4 of CaM:TFP, shows three TFP molecules binding within the hydrophobic pocket in the C-domain of CaM while one TFP molecule binds to the N-domain (Fig. 5). Literature reports have shown that the first TFP molecule binds to the C-domain. Also, the second TFP molecule binds to the hydrophobic binding site in the C-domain but not the hydrophobic binding pocket in the N-domain. Explained by a higher affinity of TFP to binding site in the C-domain rather than the binding site of the N-domain, this would be consistent with the crystal structure in which two TFP molecules bind only within the hydrophobic pocket in the C-domain [26].

In order to understand variations in the ability of the synthesized analogs to increase the intracellular Ca^{2+}, a molecular docking study was performed employing 1LIN crystal structure. After appropriate preparation of the ligands and receptor, AutoDock Vina [27] was employed to dock a set of six ligands out of the newly synthesized compounds. The docked set composed of three analogs (**3db**, **3dc** and **3dd**), whose activities are higher than TFP, as well as, three analogs (**3ab**, **3ca** and **3fa**), whose activities are lower than TFP.

The best pose calculated for the most active analogs **3db**, **3dc** and **3dd** showed docking of these analogs into the hydrophobic binding pocket in the C-domain (Fig. 6). For analogs **3db** and **3dc**, their trifluoromethyl groups were buried in the hydrophobic pocket similar to what is reported for the first molecule of TFP in 1LIN crystal structure. The docked poses showed hydrophobic interactions of the trifluoromethyl group with hydrophobic residues within the binding site. The phenothiazine moiety of analogs **3db** and **3dc** partially overlapped with the first molecule of TFP, while the increased length of the alkyl chain linker allowed situation of the morpholine or the pyrrolidine moieties of the joined cyclic amine moieties so that they overlapped with one of the phenyl rings of the second TFP molecule. Hydrophobic interactions of the linked cyclic amine moieties, as well as, π-sulfur and π-hydrophobic interactions of the phenothiazine moiety contributed to the

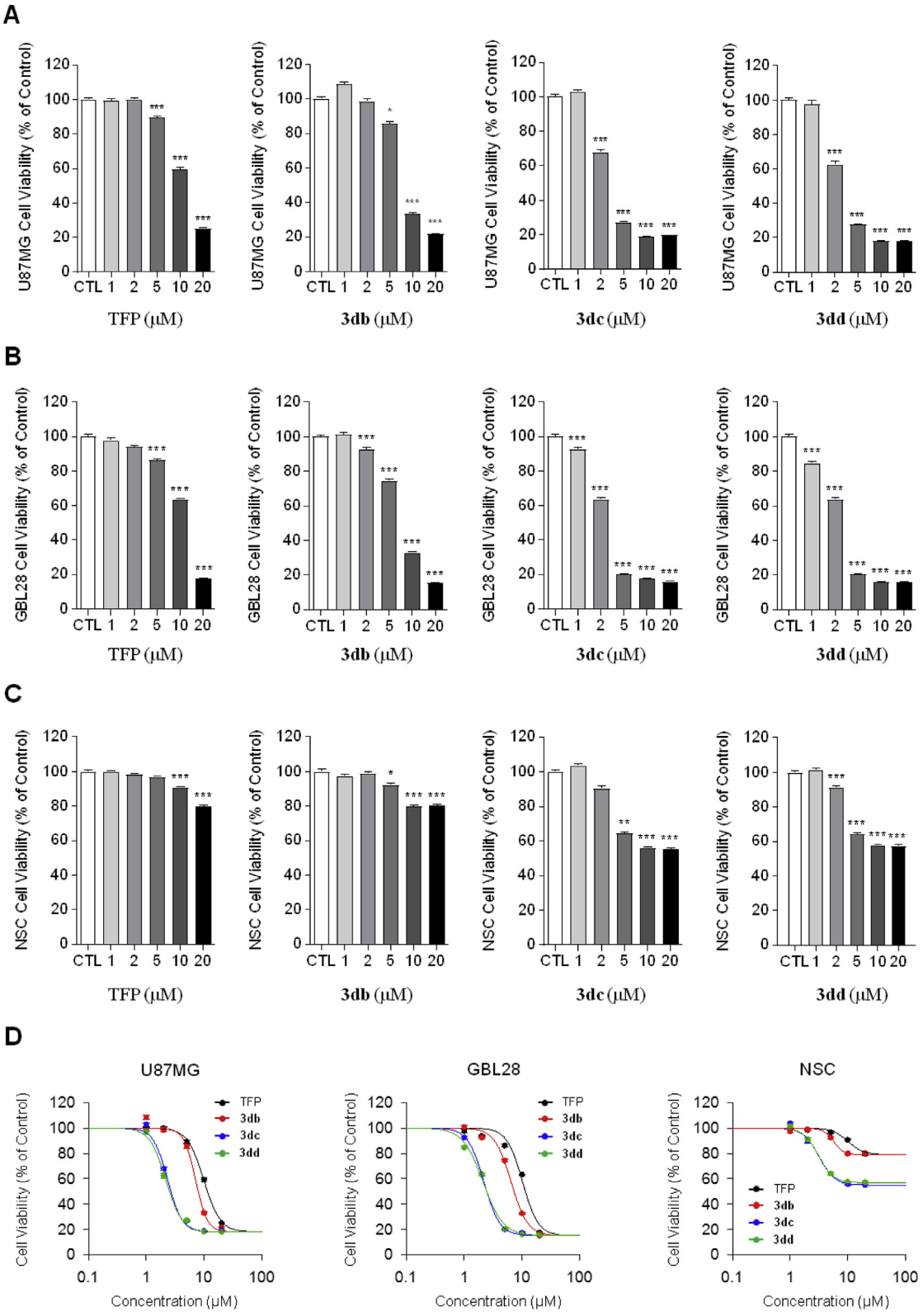

Fig. 3. MTT cell viability assay with treatment of TFP, **3db**, **3dc**, and **3dd** in U87MG, GBL28 and NSC. (A) MTT assay with TFP, **3db**, **3dc**, and **3dd** in U87MG cells ($n = 16$). Asterisk indicates a significant difference determined by one-way ANOVA ($^{*}p < 0.05$; $^{***}p < 0.001$). (B) MTT assay with TFP, **3db**, **3dc**, and **3dd** in GBL28 cells ($n = 16$). Asterisk indicates a significant difference determined by one-way ANOVA ($^{***}p < 0.001$). (C) MTT assay with TFP, **3db**, **3dc**, and **3dd** in NSCs ($n = 16$). Asterisk indicates a significant difference determined by one-way ANOVA ($^{*}p < 0.05$; $^{**}p < 0.01$; $^{***}p < 0.001$). (D) Dose response curve of TFP, **3db**, **3dc**, and **3dd** in each U87MG, GBL28 and NSC.

Table 2
Potency and efficacy of TFP, **3db**, **3dc**, and **3dd** in each U87MG glioblastoma cell, GBL28 human glioblastoma patient derived primary cell and NSC normal neural cell calculated from dose response curve.

Cell type	Potency (IC_{50} in μM)				Efficacy (%)			
	TFP	**3db**	**3dc**	**3dd**	TFP	**3db**	**3dc**	**3dd**
U87MG	9.9	7.1	2.3	2.2	82	82	82	82
GBL28	10.2	6.5	2.2	2.1	85	85	85	85
NSC	10.1	5.6	3.2	3.1	21	21	45	43

binding energetics of this pose. For analog **3dd**, the phenothiazine and the trifluoromethyl moieties overlapped with those of the second bound TFP molecule while the extended alkyl chain linker allowed the two joined cyclic amine moieties to dock in place of the phenothiazine and the trifluoromethyl moieties of the first TFP molecule. Here also, hydrophobic interactions of the joined cyclic amine moieties and the trifluoromethyl group, as well as, π-sulfur and π-hydrophobic interactions of the phenothiazine moiety contributed to the binding energetics of this pose.

The best pose calculated for analogs **3ca** and **3fa** possessing reduced activities relative to TFP showed these analogs to dock into the hydrophobic binding pocket in the C-domain (Fig. 7A and B). In contrast to analogs **3db** and **3dc** whose trifluoromethyl groups were buried into the hydrophobic pocket, the phenothiazine core of analogs **3ca** and **3fa** docked in opposite direction so that the methylthio groups are not buried into the hydrophobic pocket. For analog **3ca** the alkyl chain linker extends the cyclic amine moiety so that the methylpiperidine moiety approximates the position of the trifluoromethyl group of the second TFP molecule. In case of analog **3fa**, the docking position for the cyclic amine moiety was farther from the trifluoromethyl group of the second TFP molecule than that of analog **3ca**. The poses of analogs **3db** and **3dc** were stabilized with favorable hydrophobic interactions, as well as, π-sulfur interactions. In contrast, for analog **3ab** possessing reduced activity relative to TFP, the best pose calculated docked into the hydrophobic binding pocket in the N-domain but not the C-domain (Fig. 7C). In this pose, the phenothiazine and trifluoromethyl moieties of analog **3ab** showed interactions similar to those of TFP molecule within the hydrophobic binding site in the N-domain. However, analog **3ab** binding mode was flipped vertically so that the extended alkyl chain linker and the cyclic amine moieties were in an opposite direction to the alkyl chain linker and the methylpiperazine moieties of TFP. Accordingly, more favorable hydrophobic interactions were established between the cyclic amine moieties of analog **3ab** and amino acid residues beyond those interacting with TFP in the N-domain. This might indicate more preference of analog **3ab** to bind to the N-domain pocket rather

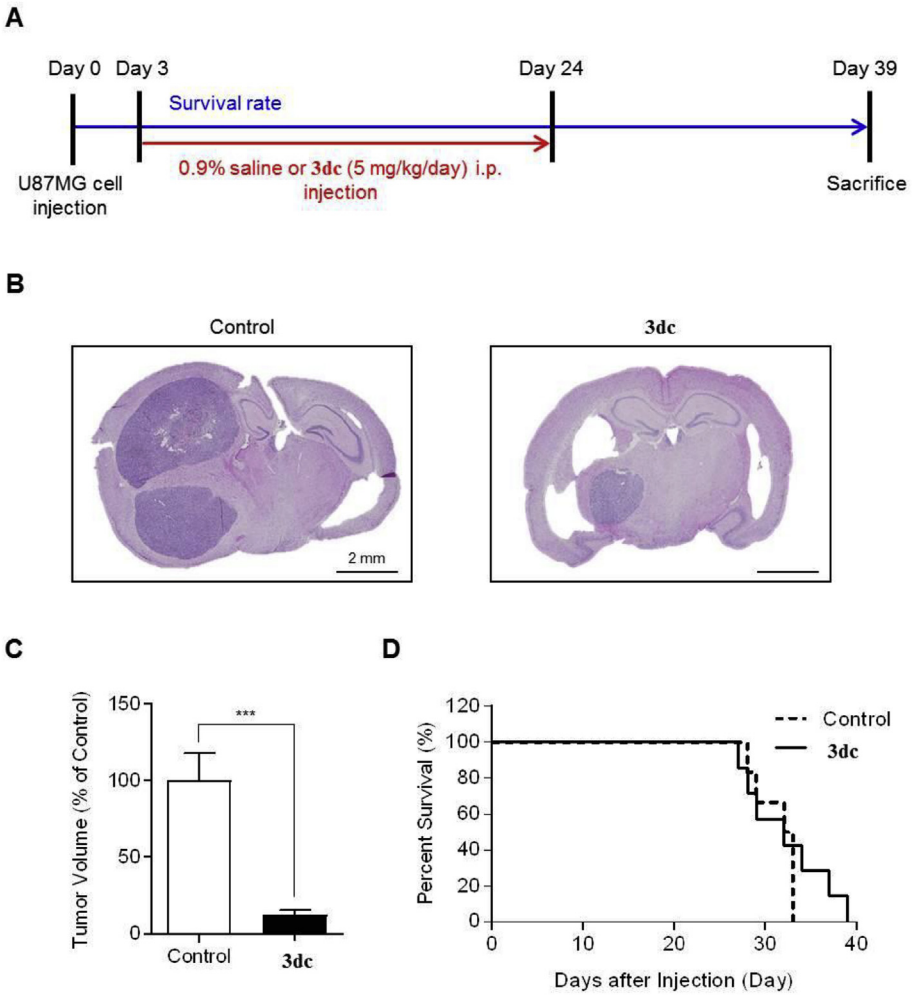

Fig. 4. Anti-glioblastoma effect of **3dc** in an *in vivo* orthotopic brain xenograft model. (A) Experimental timeline of *in vivo* orthotopic brain xenograft model in terms of saline or **3dc** treatment and survival rate of mice. (B) H&E staining of saline-treated control ($n = 10$) and **3dc**-treated ($n = 10$) mouse brain. (C) Tumor volume measured from H&E staining. Asterisk indicates a significant difference determined by unpaired two-tailed *t*-test (***$p < 0.001$). (D) Survival rate of saline-treated control and **3dc**-treated mouse.

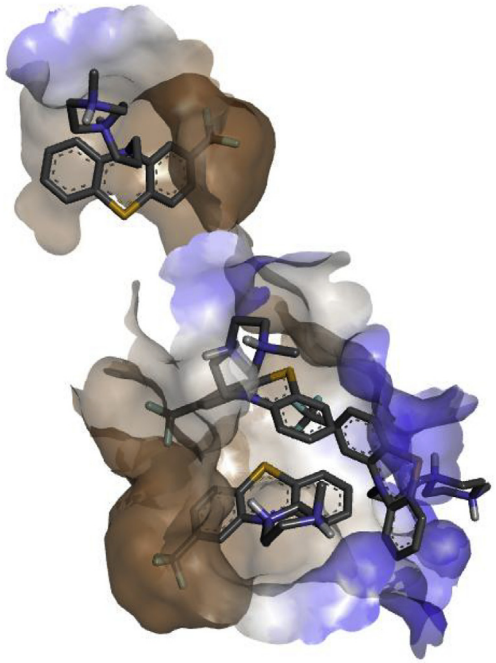

Fig. 5. Crystal structures of CaM showing three molecules of TFP binding to C-domain (lower binding pocket) and a fourth TFP molecule binding to the N-domain (upper binding pocket).

than the C-domain, and thus, might explain its reduced activity relative to TFP.

Further analysis of compounds whose best docked poses were within the hydrophobic binding site of the C-domain revealed significant differences in the calculated docking scores between the less effective analogs **3ca** and **3fa**, and the most effective analogs **3db**, **3dc** and **3dd**. It was found that the calculated docking scores for the most active analogs **3db**, **3dc** and **3dd** (−8.1, −8.0 and −8.7 for **3db**, **3dc** and **3dd** respectively) were significantly higher than those for the less active analogs **3ca** and **3fa** (−6.7 and −7.1 for **3ca** and **3fa** respectively). This wide difference in the calculated docking scores may reflect differences in affinity of these analogs to the binding pocket at the C-domain of CaM, thus, might explain differences between their elicited capabilities to produce an increased intracellular Ca^{2+} level.

3. Conclusion

In conclusion, assessment of MTT-cell viability against U87MG and GBL28 glioblastoma cell lines, as well as, the normal neural stem cells (NSCs) showed that analog **3dc** possesses a potential anti-glioblastoma effect while eliciting a reasonable selectivity to glioblastoma cells over normal neuronal stem cells. Furthermore, its *in vivo* evaluation confirmed a significant ability to reduce the brain's tumor growth in addition to increase the survival time in orthotopic brain xenograft mouse model of glioblastoma. As a whole, this work presents the novel TFP analog **3dc** as a new chemical entity that possibly could be an effective agent for adjuvant chemotherapy of glioblastoma.

4. Experimental

4.1. Chemistry

4.1.1. General methods

All reactions and manipulations were performed in nitrogen atmosphere using standard Schlenk techniques. The chemicals,

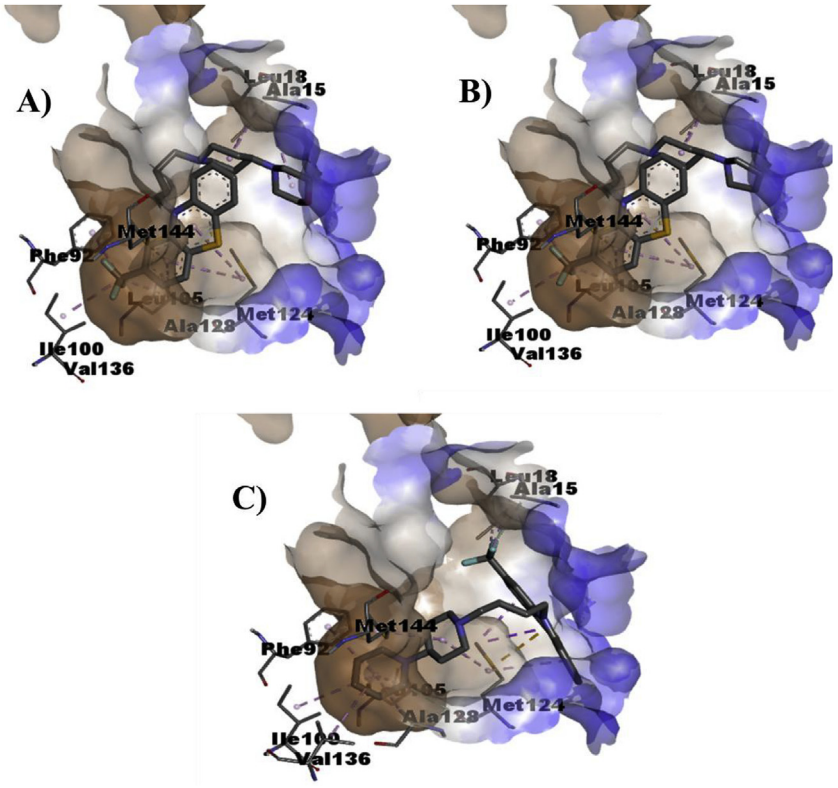

Fig. 6. Binding modes of a set of active compounds to CaM. A) Compound **3db** docked into the C-domain of CaM. B) Compound **3dc** docked into the C-domain of CaM. C) Compound **3dd** docked into the C-domain of CaM.

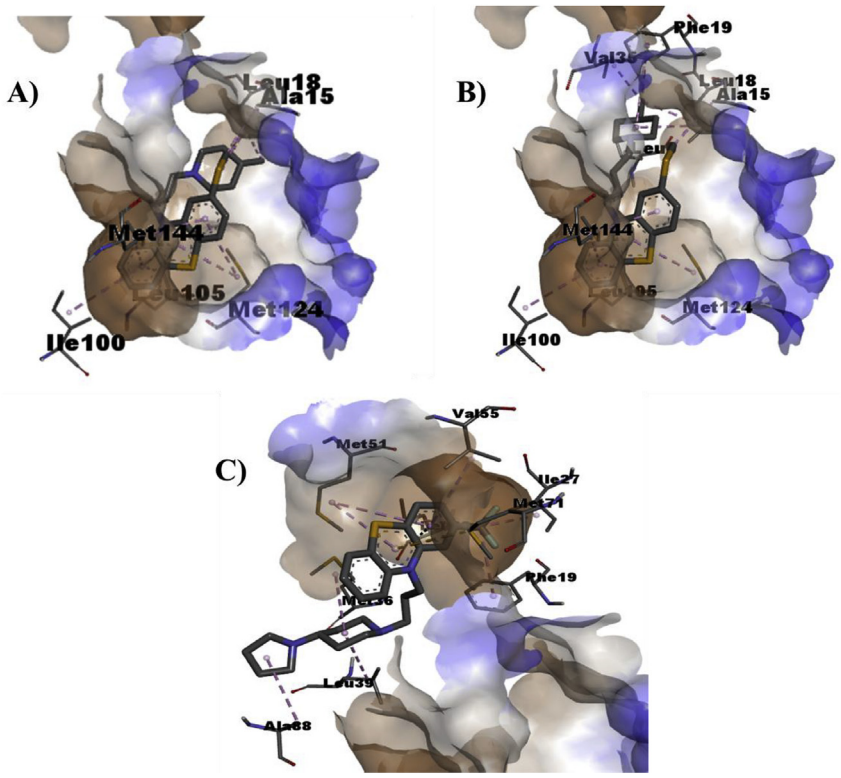

Fig. 7. Binding modes of a set of reduced activity compounds to CaM. A) Compound **3ca** docked into the C-domain of CaM. B) Compound **3fa** docked into the C-domain of CaM. C) Compound **3ab** docked into the N-domain of CaM.

reagents and reaction solvents were purchased from commercial suppliers unless otherwise mentioned and used without further purification. The NMR spectra were obtained on Bruker Avance 400 (400 MHz ^{1}H and 100.6 MHz ^{13}C NMR). ^{1}H NMR spectra were referenced to tetramethylsilane ($\delta = 0.00$ ppm) as an internal standard and were reported as follows: chemical shift, multiplicity (b = broad, s = singlet, d = doublet, t = triplet, dd = doublet of doublet, m = multiplet). Column chromatography was performed on Silica Gel 60 (230–400 mesh, Merck, Darmstadt, Germany) and eluting solvents for all of these chromatographic methods were noted as appropriated-mixed solvent with given volume-to-volume ratios. TLC was carried out using glass sheets pre-coated with silica gel 60 F_{254} purchased by Merck. The purity of samples was determined by analytical HPLC using a Water ACQUITY UPLC (CORTECS™) with C18 column (2.1 mm × 100 mm; 1.6 μm) at temperature 40 °C. HPLC data were recorded using parameters as follows: 0.1% formic acid in water and 0.1% formic acid in methanol and flow rate of 0.3 mL/min. For more details, see supplementary file. High-resolution spectra were performed on Waters ACQUITY UPLC BEH C18 1.7μ–Q-TOF SYNAPT G2-Si High Definition Mass Spectrometry.

*4.1.2. General methods of intermediates **5a**–**g***

In a sealed tube, to a solution of the appropriate phenothiazine derivative (**4a**–**d**, 3.7 mmol) in DMF (10 mL) were added NaH (60% in oil, 224.5 mg, 5.6 mmol) and 1,3- or 1,4-dihaloalkane (5.0 mmol) at 0 °C and stirred at 100 °C for 24 h. After the reaction was complete, the reaction mixture was extracted using ethyl acetate and water. The organic layer was dried over anhydrous $MgSO_4$, filtered and concentrated under reduced pressure. The residue was purified by column chromatography (EA:*n*-Hex = 1:40) to yield intermediates **5a**–**g**.

*4.1.2.1. 10-(4-Chlorobutyl)-2-(trifluoromethyl)-10H-phenothiazine (**5a**).* Yield: 50.0%, colorless oil. ^{1}H NMR (400 MHz, $CDCl_3$) δ 1.89–2.00 (m, 4H), 3.40 (d, $J = 6.0$ Hz, 1H), 3.54 (t, $J = 6.2$ Hz, 1H), 3.94 (t, $J = 6.0$ Hz, 2H), 6.89 (d, $J = 8.1$ Hz, 1H), 6.96 (t, $J = 7.4$ Hz, 1H), 7.03 (s, 1H), 7.13–7.19 (m, 2H), 7.21 (t, $J = 8.2$ Hz, 2H). ^{13}C NMR (100.6 MHz, $CDCl_3$) δ 29.73, 23.99, 44.58, 46.58, 111.96, 111.99, 116.02, 119.26, 119.30, 123.34, 124.46, 127.67, 127.74, 127.78, 130.42, 144.31, 145.68.

*4.1.2.2. 10-(3-Chloropropyl)-2-(trifluoromethyl)-10H-phenothiazine (**5b**).* Yield: 46.9%, colorless oil. ^{1}H NMR (400 MHz, $CDCl_3$) δ 2.22–2.27 (m, 1H), 2.26–2.32 (m, 1H), 3.52 (t, $J = 6.2$ Hz, 1H), 3.67 (t, $J = 6.1$ Hz, 1H), 4.11 (t, $J = 5.9$ Hz, 2H), 6.93 (d, $J = 8.1$ Hz, 1H), 6.98 (t, $J = 7.4$ Hz, 1H), 7.08 (s, 1H), 7.15–7.15 (m, 4H). ^{13}C NMR (100.6 MHz, $CDCl_3$) δ 29.45, 42.19, 44.09, 112.02, 112.06, 116.03, 119.47, 119.51, 123.47, 124.69, 127.74, 127.81, 127.82, 130.61, 144.20, 145.59.

*4.1.2.3. 2-Chloro-10-(4-chlorobutyl)-10H-phenothiazine (**5c**).* Yield: 59.7%, colorless oil. ^{1}H NMR (400 MHz, $CDCl_3$) δ 1.88–2.0 (m, 4H), 3.41 (t, $J = 6.1$ Hz, 1H), 3.54 (t, $J = 6.2$ Hz, 1H), 3.89 (t, $J = 6.4$ Hz, 2H), 6.83–6.97 (m, 4H), 7.04 (d, $J = 8.2$ Hz, 1H), 7.13–7.19 (m, 2H).

*4.1.2.4. 2-Chloro-10-(3-chloropropyl)-10H-phenothiazine (**5d**).* Yield: 63.5%, colorless oil. ^{1}H NMR (400 MHz, $CDCl_3$) δ 2.23–2.29 (m, 1H), 2.30–2.33 (m, 1H), 3.52 (t, $J = 6.2$ Hz, 1H), 3.66 (t, $J = 6.1$ Hz, 1H), 4.05 (t, $J = 6.3$ Hz, 2H), 6.87–6.92 (m, 2H), 6.94–6.98 (m, 2H), 7.05 (d, $J = 8.2$ Hz, 1H), 7.14–7.20 (m, 2H). ^{13}C NMR (100.6 MHz, $CDCl_3$) δ 29.52, 42.30, 44.06, 115.95, 115.97, 122.65, 123.26, 124.19, 125.44, 127.58, 127.76, 128.15, 133.36, 144.34, 146.41.

*4.1.2.5. 10-(4-Chlorobutyl)-2-(methylthio)-10H-phenothiazine (**5e**).* Yield: 25.6%, colorless oil. ^{1}H NMR (400 MHz, $CDCl_3$) δ 2.23–2.29

(m, 1H), 2.46 (s, 3H), 3.40 (t, $J = 6.2$ Hz, 1H), 3.53 (t, $J = 6.2$ Hz, 1H), 3.90 (t, $J = 6.3$ Hz, 2H), 6.79 (d, $J = 1.7$ Hz, 1H), 6.82–6.88 (m, 2H), 6.94 (t, $J = 6.9$ Hz, 1H), 7.06 (d, $J = 8.0$ Hz, 1H), 7.13–7.16 (m, 2H). ^{13}C NMR (100.6 MHz, $CDCl_3$) δ 16.42, 24.13, 29.83, 44.82, 46.44, 114.51, 115.88, 120.84, 122.83, 125.49, 127.41, 127.61, 127.73, 137.82, 144.84, 145.68, 171.06.

*4.1.2.6. 10-(3-Chloropropyl)-2-(methylthio)-10H-phenothiazine (**5f**).* Yield: 53.0%, colorless oil. ^{1}H NMR (400 MHz, $CDCl_3$) δ 2.23–2.27 (m, 1H), 2.29–2.32 (m, 1H), 2.46 (s, 3H), 3.50 (t, $J = 6.0$ Hz, 1H), 3.56 (t, $J = 6.1$ Hz, 1H), 4.05 (t, $J = 6.3$ Hz, 2H), 6.81–6.84 (m, 2H), 6.87–6.95 (m, 2H), 7.05 (d, $J = 8.2$ Hz, 1H), 7.13–7.17 (m, 2H). ^{13}C NMR (100.6 MHz, $CDCl_3$) δ 16.47, 29.63, 42.48, 44.04, 114.59, 115.84, 121.07, 122.60, 122.94, 125.77, 127.42, 127.68, 127.77, 137.82, 144.80, 145.56.

*4.1.2.7. 10-(4-Chlorobutyl)-2-fluoro-10H-phenothiazine (**5g**).* Yield: 95.0%, colorless oil. ^{1}H NMR (400 MHz, $CDCl_3$) δ 1.86–2.06 (m, 4H), 3.54 (t, $J = 6.2$ Hz, 2H), 3.88 (t, $J = 5.8$ Hz, 2H), 6.58–6.67 (m, 2H), 6.88 (d, $J = 8.1$ Hz, 1H), 6.95 (t, $J = 7.2$ Hz, 2H), 7.04–7.08 (m, 1H), 7.14–7.19 (m, 1H). ^{13}C NMR (100.6 MHz, $CDCl_3$) δ 24.06, 29.78, 44.72, 46.55, 103.62 ($J_{C\text{-}F} = 26.2$ Hz), 109.23 ($J_{C\text{-}F} = 22.1$ Hz), 115.83, 120.08, 120.11, 123.16, 125.38, 127.61 ($J_{C\text{-}F} = 18.1$ Hz), 128.08 ($J_{C\text{-}F} = 10.1$ Hz), 144.49, 147.03 ($J_{C\text{-}F} = 10.1$ Hz), 162.97 ($J_{C\text{-}F} = 243.5$ Hz).

*4.1.3. General methods of TFP analogs **3aa**–**ga***

To a solution of the appropriate intermediate (**5a**–**g**, 0.6 mmol) in 2-butanone were added sodium iodide (83.8 mg, 0.6 mmol), potassium carbonate (77.3 g, 0.6 mmol) and the appropriate cyclic amine derivative (0.6 mmol) and stirred at 80 °C for 24 h. After the reaction was complete, the reaction mixture was extracted with EA and water. The residue was dried over anhydrous $MgSO_4$, filtered and concentrated under reduced pressure. The residue was purified by column chromatography (DCM:MeOH = 15:1) to get the target final compounds.

*4.1.3.1. 10-(3-(Piperazin-1-yl)propyl)-2-(trifluoromethyl)-10H-phenothiazine (**3aa**).* Yield: 59.8%, colorless oil, HPLC purity: 6.06 min, 97.38%. ^{1}H NMR (400 MHz, $CDCl_3$) δ 1.21–1.37 (m, 1H), 1.86–1.96 (m, 2H), 2.52 (t, $J = 6.7$ Hz, 2H), 2.55–2.61 (m, 4H), 2.98 (s, 4H), 4.00 (t, $J = 6.5$ Hz, 2H), 6.90 (d, $J = 8.2$ Hz, 1H), 6.93–6.97 (m, 1H), 7.02 (s, 1H), 7.10–7.12 (m, 1H), 7.13–7.19 (m, 3H). HRMS (ES^+): *m/z* calculated for $C_{20}H_{22}F_3N_3S$: 394.1565 $[M+H]^+$. Found 394.1660.

*4.1.3.2. 10-(3-(4-(Pyrrolidin-1-yl)piperidin-1-yl)propyl)-2-(trifluoromethyl)-10H-phenothiazine (**3ab**).* Yield: 82.1%, white solid, HPLC purity: 5.17 min, 98.44%. ^{1}H NMR (400 MHz, $CDCl_3$) δ 1.51–1.61 (m, 2H), 1.82–1.84 (m, 5H), 1.88–1.97 (m, 5H), 2.11–2.18 (m, 1H), 2.43 (t, $J = 6.9$ Hz, 2H), 2.67 (s, 4H), 2.87 (d, $J = 11.8$ Hz, 2H), 3.94 (t, $J = 6.8$ Hz, 2H), 6.93 (t, $J = 8.1$ Hz, 2H), 7.03 (s, 1H), 7.09–7.19 (m, 4H). ^{13}C NMR (100.6 MHz, DMSO-d_6) δ 22.70, 25.24, 44.07, 50.38, 53.48, 112.10, 116.60, 119.30, 123.00, 123.50, 127.40, 127.90, 128.10, 129.60, 144.50 ($J_{C\text{-}F} = 192.0$ Hz). HRMS (ES^+): *m/z* calculated for $C_{25}H_{30}F_3N_3S$: 462.2191 $[M+H]^+$. Found 462.2244.

*4.1.3.3. 10-(3-(4-Methylpiperidin-1-yl)propyl)-2-(trifluoromethyl)-10H-phenothiazine (**3ac**).* Yield: 68.7%, white solid, HPLC purity: 6.08 min, 100%. ^{1}H NMR (400 MHz, $CDCl_3$) δ 0.90 (s, 3H), 1.14–1.21 (m, 2H), 1.26–1.35 (m, 1H), 1.60 (d, $J = 12.0$ Hz, 2H), 1.85–1.98 (m, 4H), 2.46 (t, $J = 6.7$ Hz, 2H), 2.83 (d, $J = 12.0$ Hz, 2H), 4.00 (t, $J = 8.0$ Hz, 2H), 6.91–6.95 (m, 2H), 7.03 (s, 1H), 7.09–7.11 (m, 1H), 7.14 (s, 1H), 7.16–7.19 (m, 2H). ^{13}C NMR (100.6 MHz, $CDCl_3$) δ 20.86, 21.09, 29.29, 30.73, 44.78, 53.23, 55.25, 112.31, 116.60, 119.78, 119.81, 122.59, 123.91, 125.03, 127.90, 128.14, 130.14, 130.97, 143.45, 145.53. HRMS (ES^+): *m/z* calculated for $C_{22}H_{25}F_3N_2S$: 407.1769 $[M+H]^+$. Found 407.1818.

*4.1.3.4. 2-Chloro-10-(3-(4-methylpiperidin-1-yl)propyl)-10H-phenothiazine (**3ba**).* Yield: 39.1%, brown solid, HPLC purity: 5.95 min, 99.83%. ^{1}H NMR (400 MHz, $CDCl_3$) δ 0.91 (d, $J = 8.0$ Hz, 3H), 1.28–1.35 (m, 3H), 1.60 (d, $J = 12.0$ Hz, 2H), 1.86–1.92 (m, 2H), 1.93–1.98 (m, 2H), 2.44 (t, $J = 6.8$ Hz, 2H), 2.85 (d, $J = 12.0$ Hz, 2H) 4.00 (t, $J = 6.9$ Hz, 2H), 6.84–6.93 (m, 4H), 6.99–7.00 (m, 1H) 7.09–7.16 (m, 2H). ^{13}C NMR (100.6 MHz, $CDCl_3$) δ 20.89, 21.18, 29.19, 30.75, 44.70, 53.22, 55.21, 116.28, 116.50, 122.99, 123.63, 124.43, 125.65, 127.80, 127.90, 128.23, 133.57, 143.72, 146.17. HRMS (ES^+): *m/z* calculated for $C_{21}H_{25}ClN_2S$: 373.1505 $[M+H]^+$. Found 373.1573.

*4.1.3.5. 10-(3-(4-Methylpiperidin-1-yl)propyl)-2-(methylthio)-10H-phenothiazine (**3ca**).* Yield: 44.9%, yellow solid, HPLC purity: 5.97 min, 100%. ^{1}H NMR (400 MHz, $CDCl_3$) δ 0.90 (d, $J = 6.4$ Hz, 3H), 1.17–1.26 (m, 2H), 1.27–1.33 (m, 1H), 1.59 (d, $J = 12.6$ Hz, 2H), 1.83–1.89 (m, 2H), 1.90–1.98 (m, 2H), 2.43 (t, $J = 7.3$ Hz, 2H), 2.44 (s, 3H), 2.83 (d, $J = 11.6$ Hz, 2H), 3.89 (t, $J = 6.9$ Hz, 2H), 6.78–6.81 (m, 2H), 6.87–6.90 (m, 2H), 7.00–7.03 (m, 1H), 7.09–7.14 (m, 2H). ^{13}C NMR (100.6 MHz, $CDCl_3$) δ 16.54, 21.95, 24.65, 30.82, 34.37, 45.62, 54.21, 56.24, 114.62, 115.76, 120.78, 122.04, 122.53, 125.05, 127.24, 127.41, 127.51, 137.51, 144.93, 145.75. HRMS (ES^+): *m/z* calculated for $C_{22}H_{28}N_2S_2$: 385.1772 $[M+H]^+$. Found 385.1775.

*4.1.3.6. 10-(4-(4-Methylpiperidin-1-yl)butyl)-2-(trifluoromethyl)-10H-phenothiazine (**3da**).* Yield: 93.4%, yellow solid, HPLC purity: 6.18 min, 99.48%. ^{1}H NMR (400 MHz, $CDCl_3$) δ 0.89–0.93 (m, 3H), 1.14–1.25 (m, 3H), 1.29–1.33 (m, 2H), 1.63–1.66 (m, 2H), 1.79–1.87 (m, 4H), 2.33 (t, $J = 7.4$ Hz, 2H), 2.84 (d, $J = 11.4$ Hz, 2H), 3.91 (t, $J = 7.1$ Hz, 2H), 6.91 (d, $J = 8.2$ Hz, 1H), 6.92–6.96 (m, 1H), 7.01 (s, 1H), 7.10–7.12 (m, 1H), 7.15–7.20 (m, 4H). ^{13}C NMR (100.6 MHz, $CDCl_3$) δ 20.90, 20.93, 23.89, 29.43, 30.75, 46.38, 52.95, 56.91, 112.20, 112.24, 116.38, 119.51, 119.55, 123.62, 124.63, 127.80, 127.81, 128.00, 129.72, 130.04, 130.56. HRMS (ES^+): *m/z* calculated for $C_{23}H_{27}F_3N_2S$: 421.1925 $[M+H]^+$. Found 421.2000.

*4.1.3.7. 4-(1-(4-(2-(Trifluoromethyl)-10H-phenothiazin-10-yl)butyl) piperidin-4-yl)morpholine (**3db**).* Yield: 76.0%, white solid, HPLC purity: 5.44 min, 99.05%. ^{1}H NMR (400 MHz, $CDCl_3$) δ 1.54–1.56 (m. 2H), 1.64–1.66 (m, 4H), 1.77–1.91 (m, 6H), 2.16–2.19 (m, 1H), 2.52 (t, $J = 4.4$ Hz, 4H), 2.95 (d, $J = 10.2$ Hz, 2H), 3.71 (t, $J = 4.6$ Hz, 4H), 3.91 (t, $J = 6.9$ Hz, 2H), 6.89 (d, $J = 8.1$ Hz, 1H), 6.93–6.97 (m, 1H), 7.11–7.21 (m, 4H). ^{13}C NMR (100.6 MHz, $CDCl_3$) δ 24.09, 24.59, 27.90, 47.26, 49.71, 53.01, 57.75, 62.17, 67.35, 111.83, 111.87, 115.90, 119.01, 122.83, 123.08, 124.09, 127.47, 127.56, 127.62, 129.55, 129.74, 129.98. HRMS (ES^+): *m/z* calculated for $C_{26}H_{32}F_3N_3OS$: 492.2218 $[M+H]^+$. Found 492.2299.

*4.1.3.8. 10-(4-(4-(Pyrrolidin-1-yl)piperidin-1-yl)butyl)-2-(trifluoromethyl)-10H-phenothiazine (**3dc**).* Yield: 68.0%, white solid, HPLC purity: 5.30 min, 98.29%. ^{1}H NMR (400 MHz, $CDCl_3$) δ 1.47–1.58 (m, 2H), 1.59–1.65 (m, 2H), 1.77–1.86 (m, 8H), 1.89–1.91 (m, 2H), 1.94–1.98 (m, 1H), 2.31 (t, $J = 7.2$ Hz, 2H), 2.56 (s, 4H), 2.86 (d, $J = 11.4$ Hz, 2H), 3.89 (t, $J = 6.9$ Hz, 2H), 6.88–6.95 (m, 2H), 7.01 (s, 1H), 7.10–7.19 (m, 4H). ^{13}C NMR (100.6 MHz, DMSO-d_6) δ 21.24, 23.20, 24.14, 25.55, 46.56, 50.24, 50.97, 55.71, 58.42, 112.53, 117.08, 119.62, 123.30, 123.53, 123.85, 126.01, 127.92, 128.38, 128.53, 130.10, 144.28, 146.01. HRMS (ES^+): *m/z* calculated for $C_{26}H_{32}F_3N_3S$: 476.2347 $[M+H]^+$. Found 476.2388.

*4.1.3.9. 10-(4-([1,4′-Bipiperidin]-1′-yl)butyl)-2-(trifluoromethyl)-10H-phenothiazine (**3dd**).* Yield: 21.0%, white solid, HPLC purity: 5.31 min, 98.26%. ^{1}H NMR (400 MHz, DMSO-d_6) δ 1.39–1.42 (m, 2H), 1.69–1.75 (m, 4H), 1.77–1.82 (m, 6H), 2.03–2.09 (m, 3H), 2.26–2.33

(m, 2H), 2.87–2.92 (m, 4H), 2.99–3.05 (m, 2H), 3.56 (d, $J = 8.3$ Hz, 2H), 4.00 (t, $J = 6.5$ Hz, 2H), 7.03 (t, $J = 7.4$ Hz, 1H), 7.10 (d, $J = 7.9$ Hz, 1H), 7.21–7.23 (m, 1H), 7.24–7.27 (m, 2H), 7.29–7.31 (m, 1H), 7.40 (d, $J = 8.0$ Hz, 1H), 10.14 (s, 1H), 10.44 (s, 1H). ^{13}C NMR (100.6 MHz, MeOD) δ 21.25, 21.34, 22.96, 23.40, 23.82, 46.00, 50.21, 50.52, 56.24, 60.02, 111.88, 111.92, 116.35, 119.02, 119.06, 123.27, 124.51, 127.26, 127.51, 127.75, 130.86, 144.22, 146.04. HRMS (ES^+): *m/z* calculated for $C_{27}H_{34}F_3N_3S$: 490.2504 $[M+H]^+$. Found 490.2536.

*4.1.3.10. 10-(4-(4-Phenylpiperazin-1-yl)butyl)-2-(trifluoromethyl)-10H-phenothiazine (**3de**).* Yield: 63.0%, white solid, HPLC purity: 6.34 min, 100%. ^{1}H NMR (400 MHz, $CDCl_3$) δ 1.63–1.70 (m, 2H), 1.83–1.90 (m, 2H), 2.40 (t, $J = 7.1$ Hz, 2H), 2.53 (t, $J = 4.9$ Hz, 4H), 3.14 (t, $J = 4.7$ Hz, 4H), 3.91 (t, $J = 6.9$ Hz, 2H), 6.84 (t, $J = 7.3$ Hz, 1H), 6.89–6.96 (m, 4H), 7.02 (s, 1H), 7.11–7.20 (m, 4H), 7.23–7.27 (m, 2H). ^{13}C NMR (100.6 MHz, $CDCl_3$) δ 22.83, 24.47, 47.24, 49.10, 53.18, 57.81, 111.85, 111.89, 115.96, 116.05, 119.05, 119.09, 119.67, 123.13, 124.14, 127.51, 127.60, 127.65, 128.28, 129.11, 144.39, 145.74, 151.35. HRMS (ES^+): *m/z* calculated for $C_{27}H_{28}F_3N_3S$: 484.2034 $[M+H]^+$. Found 484.2022.

*4.1.3.11. 10-(4-(4-Methyl-1,4-diazepan-1-yl)butyl)-2-(trifluoromethyl)-10H-phenothiazine (**3df**).* Yield: 93.4%, brown oil, HPLC purity: 5.47 min, 91.38%. ^{1}H NMR (400 MHz, $CDCl_3$) δ 1.59–1.66 (m, 2H), 1.79–1.88 (m, 2H), 1.91–1.97 (m, 2H), 2.52 (s, 3H), 2.60 (t, $J = 7.1$ Hz, 2H), 2.73 (t, $J = 6.1$ Hz, 2H), 2.75–2.78 (m, 4H), 2.88 (t, $J = 5.5$ Hz, 2H), 3.93 (t, $J = 6.6$ Hz, 2H), 6.90 (d, $J = 8.1$ Hz, 1H), 6.97 (t, $J = 7.5$ Hz, 1H), 7.02 (s, 1H), 7.11–7.15 (m, 2H), 7.16–7.21 (m, 2H). HRMS (ES^+): *m/z* calculated for $C_{23}H_{28}F_3N_3S$: 436.2034 $[M+H]^+$. Found 436.2117.

*4.1.3.12. 2-Fluoro-10-(4-(4-methylpiperidin-1-yl)butyl)-10H-phenothiazine (**3ea**).* Yield: 72.9%, white solid, HPLC purity: 5.84 min, 92.05%. ^{1}H NMR (400 MHz, $CDCl_3$) δ 0.90 (d, $J = 6.3$ Hz, 3H), 1.17–1.26 (m, 2H), 1.27–1.37 (m, 1H), 1.57–1.66 (m, 4H), 1.78–1.88 (m, 4H), 2.32 (t, $J = 7.4$ Hz, 2H), 2.84 (d, $J = 11.6$ Hz, 2H), 3.82 (t, $J = 7.2$ Hz, 2H), 6.59–6.63 (m, 2H), 6.93 (d, $J = 8.4$ Hz, 1H). ^{13}C NMR (100.6 MHz, MeOD) δ 19.98, 21.10, 23.45, 28.49, 31.11, 45.98, 52.66, 56.41, 103.53 ($J_{C\text{-}F} = 26.2$ Hz), 108.86 ($J_{C\text{-}F} = 22.1$ Hz), 116.05, 120.33, 122.96, 125.43, 127.13, 127.40, 127.75 ($J_{C\text{-}F} = 10.1$ Hz), 144.49, 147.30 ($J_{C\text{-}F} = 9.1$ Hz), 163.07 ($J_{C\text{-}F} = 243.5$ Hz). HRMS (ES^+): *m/z* calculated for $C_{22}H_{27}FN_2S$: 371.1957 $[M+H]^+$. Found 371.2009.

*4.1.3.13. 10-(4-(4-Methylpiperidin-1-yl)butyl)-2-(methylthio)-10H-phenothiazine (**3fa**).* Yield: 59.7%, yellowish white solid, HPLC purity: 6.09 min, 99.30%. ^{1}H NMR (400 MHz, $CDCl_3$) δ 0.90 (d, $J = 6.3$ Hz, 3H), 1.15–1.25 (m, 2H), 1.27–1.34 (m, 1H), 1.56–1.65 (m, 4H), 1.77–1.87 (m, 4H), 2.32 (t, $J = 7.3$ Hz, 2H), 2.45 (s, 3H), 2.84 (d, $J = 11.6$ Hz, 2H), 3.86 (t, $J = 7.1$ Hz, 2H), 6.77–6.81 (m, 2H), 6.86–6.91 (m, 2H), 7.03 (d, $J = 7.9$ Hz, 1H), 7.09–7.14 (m, 2H). ^{13}C NMR (100.6 MHz, $CDCl_3$) δ 16.34, 20.94, 23.86, 27.09, 29.31, 30.76, 46.21, 52.85, 56.84, 114.67, 116.24, 121.05, 122.37, 123.06, 125.68, 127.58, 127.64, 127.75, 138.13, 144.59, 145.60. HRMS (ES^+): *m/z* calculated for $C_{23}H_{30}N_2S_2$: 399.1928 $[M+H]^+$. Found 399.1951.

*4.1.3.14. 2-Chloro-10-(4-(4-(pyrrolidin-1-yl)piperidin-1-yl)butyl)-10H-phenothiazine (**3ga**).* Yield: 72.5%, white solid, HPLC purity: 5.14 min, 93.76%. ^{1}H NMR (400 MHz, DMSO-d_6) δ 1.71–1.78 (m, 4H), 1.87–1.90 (m, 2H), 1.97–1.99 (m, 3H), 2.04–2.14 (m, 2H), 2.22–2.25 (m, 2H), 2.82–2.86 (m, 2H), 3.03 (s, 4H), 3.49–3.55 (m, 4H), 4.00 (t, $J = 7.8$ Hz, 2H), 6.98–7.03 (m, 2H), 7.06–7.10 (m, 2H), 7.17–7.20 (m, 2H), 7.22–7.26 (m, 1H). ^{13}C NMR (100.6 MHz, MeOD) δ 21.23, 22.52, 23.36, 45.92, 51.79, 58.61, 115.89, 116.20, 122.29, 123.03, 124.28, 125.24, 127.19, 127.51, 127.80, 133.27, 144.45, 146.78. HRMS (ES^+): *m/z* calculated for $C_{25}H_{32}ClN_3S$: 442.2083 $[M+H]^+$. Found 442.2075.

4.2. Biological evaluation

4.2.1. General statistical analysis

When two groups were being compared, the significance of data was assessed by the two-tailed Student's unpaired *t*-test using Microsoft Excel software. Other statistical analysis was done using GraphPad Prism for Windows (version 5.0, GraphPad Software, La Jolla, CA, USA). Differences between three or more means were determined by one-way ANOVA with Dunnett's multiple comparison test or Dunn's multiple comparison test. For comparing Ca^{2+} response in each U87MG or NSC group as well as between U87MG and NSC group (Fig. 2C), two-way ANOVA with Sidak's multiple comparisons test was performed for statistical analysis. Dose response curve of Ca^{2+} response was made by non-linear regression according to the equation of Sigmoidal and Logistic with 4 parameters. Linear mixed effects regression models were used to estimate and compare the group-specific change in tumor growth curves. Differences in survival curves were determined by Log-Rank test. The statistical analysis was performed at the $p < 0.05$ level of significance.

4.2.2. Cell lines and culture

U87MG human glioblastoma cells were obtained from the American Type Culture Collection (ATCC, Manassas, VA, USA) in 2006. Human primary glioblastoma (GBL) cell lines (GBL28) and neural stem cells (NSCs) were generated from the Seoul National University Hospital (Seoul, Korea, IRB No; H-0507-509-153). All cell lines have originated from the human neuronal system. The followings are the characteristics of GBL-28 glioblastoma multiforme. In morphometric analysis, Ki-67 is positive in 2.24% (2032/9056) and p53 is positive in 75.1% (734/977) of tumor cells. In immunochemical analysis, Glial fibrillary acidic protein is positive, EGFR is positive (+++/3), EGFR VIII is negative (-/3), p53 is positive, PTEN is positive (No loss), MGMT is heterogeneously positive, Galectin 3 is negative, Synaptophysin is negative, and IDH-1 is negative. NSCs were generated from brain cortex of normal brain. This cell line differentiates into neural progenitor cells in condition of neural stem culture system. Cells were cultured under conditions of 5% CO_2 and air humidified in a 37 °C incubator. Culture media were DMEM (Corning Costa, NY, USA) containing 10% fetal bovine serum, 100 U/mL penicillin and 100 μg/mL streptomycin (Gibco Invitrogen, Grand Island, NY, USA). Each cell line was stocked at early passages and cultures were maintained until passage 20 (within 2 months).

4.2.3. Ca^{2+} imaging

U87MG human glioblastoma cells were incubated with 5 μM Fura-2 AM plus 1 μM pluronic acid (Molecular Probes) for 40 min at room temperature. External solution contained 150 NaCl, 10 HEPES, 3KCl, 2 $CaCl_2$, 2 $MgCl_2$, 5.5 glucose (in mM), adjusted to pH 7.3 and osmolarity to 325 mOsmol kg^{-1}. Intensity images of 510 nm wavelength were taken at 340 nm and 380 nm excitation wavelengths using iXon EMCCD (DV887 DCS-BV, ANDOR technology, Belfast, UK) under the condition with bath application of several concentration (1, 3, 10, 30 and 100 μM) of TFP and the tested TFP analogs. The two resulting images were used for ratio calculations in Axon Imaging Workbench version 6.2 (Axon Instruments). For comparing the Ca^{2+} response, we measured the peak amplitude of Ca^{2+} imaging trace after the starting time of drug application from the baseline (0–50 s).

4.2.4. In vitro cell viability

Cells were seeded into 96-well plates at a density of 1.5×10^3 cells/well and allowed to attach to the plate for 24 h. Cells were treated with vehicle or the indicated concentrations of TFP (Sigma, St. Louis, MO, USA) and synthesized TFP analogs diluted in

complete media for 24 h. Cell viability was determined by 3-[4,5-dimethylthiazol-2-yl]-2,5-diphenyltetrazolium bromide (MTT) assay. After treatment of TFP and TFP analogs, 100 μL of 1× MTT (Amresco, Solon, OH, USA) labeling reagent was added to each well and cells were incubated for additional 2 h. The proliferative activity or viability was calculated as the relative percentage of cell numbers at initial time.

4.2.5. In vivo study with brain xenograft

In the brain xenograft model, an orthotopic implantation model was established as previously mentioned [5]. Briefly, at the third day after U87MG cells (5 μL, 2.5×10^5 cells) injection in the left frontal lobe at coordinates 2 mm lateral from the bregma, 0.5 mm anterior, and 3.5 mm intraparenchymal, **3dc** was given as intraperitoneal injection (5 mg/kg/day) ($n = 10$). The control animals were given 0.9% saline ($n = 10$). A total of 21 days treatments were given, with a 24 h rest period. Mice were monitored daily for their general appearance, behavioral changes, and neurologic deficits. Mice were sacrificed when moribund. All animals were euthanized and autopsied. Brains were collected and fixed by 4% paraformaldehyde in phosphate buffered saline. All protocols were approved by the Gyeongsang National University Institutional Animal Care and Use Committee.

4.2.6. Histopathological examination

For checking tumor size in the brain, mouse brain tissues were stained with hematoxylin and eosin. For H&E staining, the fixed tumors were embedded in paraffin, cut into 5 μm, and stained with H&E. Slides were photographed using an optical or confocal microscope (BX61VS, Olympus, Hamburg, Germany). Tumor volume (mm^3) was measured by the equation of [major axis · (minor axis of tumor)^2]/2.

4.2.7. Molecular modeling study

For molecular docking simulation, six compounds were sketched, hydrogens added, minimized and Gasteiger charges were calculated for the minimized structures. The protein crystal structure was downloaded from protein data bank and prepared for docking. Protein preparation steps included deleting all solvent molecules, removing the ligand, adding hydrogens and calculating charges of standard residues using AMBER ff14 S B forcefield and Gasteiger charges for other residues. AutoDock Vina 1.1.2 [27] was used to generate the docked poses within a window of maximum energy difference of 3 kcal/mol and a search cube size of $35 \times 35 \times 35$ Å which encloses the four TFP-binding sites. The top ten scored poses were retrieved and analyzed.

Conflicts of interest

The authors declare no potential conflict of interest.

Acknowledgement

This study was supported by the KIST Institutional programs (Grant No. 2E28010) from Korea Institute of Science and Technology (to E.J. Roh), the Creative Fusion Research Program through the Creative Allied Project funded by the National Research Council of Science & Technology (CAP-12-1-KIST) (to E.J. Roh), the National Research Foundation of Korea (NRF), a grant funded by the Korean Government (MEST) (2013R1A2A2A01068964) (to S.S. Kang), the Creative Research Initiative Program, the Korean National Research Foundation (2015R1A3A2066619) (to C.J. Lee), the KU-KIST Graduate School of Science and Technology program (R1435283) (to C.J. Lee), KIST Institutional Grant (2E26860) (to C.J. Lee), the Korea Healthcare Technology R&D Project funded by the Ministry of Health & Welfare (grant no. HI11C21100200) (to S.H. Paek), the Technology Innovation Program funded by the Ministry of Trade, Industry & Energy (grant no. 10050154, Business Model Development for Personalized Medicine Based on Integrated Genome and Clinical Information) (to S.H. Paek), and the Bio & Medical Technology Development Program of the NRF funded by the Korean government (MSIP) (grant no. 2015M3C7A1028926) (to S.H. Paek).

Appendix A. Supplementary data

Supplementary data related to this article can be found at https://doi.org/10.1016/j.ejmech.2018.03.055.

References

[1] A. Eramo, L. Ricci-Vitiani, A. Zeuner, R. Pallini, F. Lotti, G. Sette, E. Pilozzi, L.M. Larocca, C. Peschle, R. De Maria, Chemotherapy resistance of glioblastoma stem cells, Cell Death Differ. 13 (2006) 1238–1241.
[2] X. Yuan, J. Curtin, Y. Xiong, G. Liu, S. Waschsmann-Hogiu, D.L. Farkas, K.L. Black, J.S. Yu, Isolation of cancer stem cells from adult glioblastoma multiforme, Oncogene 23 (2004) 9392–9400.
[3] D.S. Nørøxe, H.S. Poulsen, U. Lassen, Hallmarks of glioblastoma: a systematic review, ESMO Open 1 (2017) e000144.
[4] S.S. Kang, K.S. Han, B.M. Ku, Y.K. Lee, J. Hong, H.Y. Shin, A.G. Almonte, D.H. Woo, D.J. Brat, E.M. Hwang, S.H. Yoo, C.K. Chung, S.H. Park, S.H. Paek, E.J. Roh, S.J. Lee, J.Y. Park, S.F. Traynelis, C.J. Lee, Caffeine-mediated inhibition of calcium release channel inositol 1,4,5-trisphosphate receptor subtype 3 blocks glioblastoma invasion and extends survival, Canc. Res. 70 (2010) 1173–1183.
[5] S. Kang, J. Hong, J.M. Lee, H.E. Moon, B. Jeon, J. Choi, N.A. Yoon, S.H. Paek, E.J. Roh, C.J. Lee, S.S. Kang, Trifluoperazine, a well-known antipsychotic, inhibits glioblastoma invasion by binding to calmodulin and disinhibiting calcium release channel IP3R, Mol. Canc. Ther. 16 (2017) 217–227.
[6] R. Stupp, M.E. Hegi, W.P. Mason, M.J. van den Bent, M.J. Taphoorn, R.C. Janzer, S.K. Ludwin, A. Allgeier, B. Fisher, K. Belanger, P. Hau, A.A. Brandes, J. Gijtenbeek, C. Marosi, C.J. Vecht, K. Mokhtari, P. Wesseling, S. Villa, E. Eisenhauer, T. Gorlia, M. Weller, D. Lacombe, J.G. Cairncross, R.O. Mirimanoff, R. European Organisation for, T. Treatment of Cancer Brain, G. Radiation Oncology, G. National Cancer Institute of Canada Clinical Trials, Effects of radiotherapy with concomitant and adjuvant temozolomide versus radiotherapy alone on survival in glioblastoma in a randomised phase III study: 5-year analysis of the EORTC-NCIC trial, Lancet Oncol. 10 (2009) 459–466.
[7] P.D. Delgado-Lopez, E.M. Corrales-Garcia, Survival in glioblastoma: a review on the impact of treatment modalities, Clin. Transl. Oncol. 18 (2016) 1062–1071.
[8] S. Ishiuchi, K. Tsuzuki, Y. Yoshida, N. Yamada, N. Hagimura, H. Okado, A. Miwa, H. Kurihara, Y. Nakazato, M. Tamura, T. Sasaki, S. Ozawa, Blockage of Ca(2+)-permeable AMPA receptors suppresses migration and induces apoptosis in human glioblastoma cells, Nat. Med. 8 (2002) 971–978.
[9] D.N. Louis, Molecular pathology of malignant gliomas, Annu. Rev. Pathol. 1 (2006) 97–117.
[10] A. Ghose, G. Lim, S. Husain, Treatment for glioblastoma multiforme: current guidelines and Canadian practice, Curr. Oncol. 17 (2010) 52–58.
[11] H.S. Friedman, T. Kerby, H. Calvert, Temozolomide and treatment of malignant glioma, Clin. Canc. Res. 6 (2000) 2585–2597.
[12] S.Y. Lee, Temozolomide resistance in glioblastoma multiforme, Genes Dis. 3 (2016) 198–210.
[13] G. Perazzoli, J. Prados, R. Ortiz, O. Caba, L. Cabeza, M. Berdasco, B. Gonzalez, C. Melguizo, Temozolomide resistance in glioblastoma cell lines: implication of MGMT, MMR, P-glycoprotein and CD133 expression, PLoS One 10 (2015) e0140131.
[14] R.J. Komotar, M.L. Otten, G. Moise, E.S. Connolly Jr., Radiotherapy plus concomitant and adjuvant temozolomide for glioblastoma-a critical review, Clin. Med. Oncol. 2 (2008) 421–422.
[15] S.M. Chang, P. Theodosopoulos, K. Lamborn, M. Malec, J. Rabbitt, M. Page, M.D. Prados, Temozolomide in the treatment of recurrent malignant glioma, Cancer 100 (2004) 605–611.
[16] T.M. Yang, H.C. Wang, Y.J. Lin, W.C. Lin, C.H. Lu, W.N. Chang, H.W. Chang, J.T. Ho, Radiotherapy followed by adjuvant temozolomide treatment of malignant glioma, Surg. Neurol. 70 (Suppl. 1) (2008) 60–63. S1.
[17] M. Westphal, K. Lamszus, The neurobiology of gliomas: from cell biology to the development of therapeutic approaches, Nat. Rev. Neurosci. 12 (2011) 495–508.
[18] T.T. Ashburn, K.B. Thor, Drug repositioning: identifying and developing new uses for existing drugs, Nat. Rev. Drug Discov. 3 (2004) 673–683.
[19] A.S. Brown, C.J. Patel, A standard database for drug repositioning, Sci. Data 4 (2017) 170029.
[20] E.L. Tobinick, The value of drug repositioning in the current pharmaceutical market, Drug News Perspect. 22 (2009) 119–125.

[21] C.T. Yeh, A.T. Wu, P.M. Chang, K.Y. Chen, C.N. Yang, S.C. Yang, C.C. Ho, C.C. Chen, Y.L. Kuo, P.Y. Lee, Y.W. Liu, C.C. Yen, M. Hsiao, P.J. Lu, J.M. Lai, L.S. Wang, C.H. Wu, J.F. Chiou, P.C. Yang, C.Y. Huang, Trifluoperazine, an antipsychotic agent, inhibits cancer stem cell growth and overcomes drug resistance of lung cancer, Am. J. Respir. Crit. Care Med. 186 (2012) 1180–1188.
[22] G.T. Budd, R.M. Bukowski, A. Lichtin, L. Bauer, P. Van Kirk, R. Ganapathi, Phase II trial of doxorubicin and trifluoperazine in metastatic breast cancer, Invest. N. Drugs 11 (1993) 75–79.
[23] J.R. Murren, H.J. Durivage, A.C. Buzaid, M. Reiss, S.D. Flynn, D. Carter, W.N. Hait, Trifluoperazine as a modulator of multidrug resistance in refractory breast cancer, Canc. Chemother. Pharmacol. 38 (1996) 65–70.
[24] S. Naftalovich, E. Yefenof, Y. Eilam, Antitumor effects of ketoconazole and trifluoperazine in murine T-cell lymphomas, Canc. Chemother. Pharmacol. 28 (1991) 384–390.
[25] M.D. Feldkamp, L. Gakhar, N. Pandey, M.A. Shea, Opposing orientations of the anti-psychotic drug trifluoperazine selected by alternate conformations of M144 in calmodulin, Proteins 83 (2015) 989–996.
[26] N. Yamaotsu, M. Suga, S. Hirono, Molecular dynamics simulation of the calmodulin-trifluoperazine complex in aqueous solution, Biopolymers 58 (2001) 410–421.
[27] O. Trott, A.J. Olson, AutoDock Vina: improving the speed and accuracy of docking with a new scoring function, efficient optimization, and multi-threading, J. Comput. Chem. 31 (2010) 455–461.